

Cite this: *Lab Chip*, 2011, **11**, 2343

www.rsc.org/loc

PAPER

Feedback control system simulator for the control of biological cells in microfluidic cross slots and integrated microfluidic systems†

Michael D. Curtis,^a Gregory J. Sheard^b and Andreas Fouras^{*a}

Received 3rd March 2011, Accepted 9th May 2011

DOI: 10.1039/c1lc20191c

Control systems for lab on chip devices require careful characterisation and design for optimal performance. Traditionally, this involves either extremely computationally expensive simulations or lengthy iteration of laboratory experiments, prototype design, and manufacture. In this paper, an efficient control simulation technique, valid for typical microchannels, Computed Interpolated Flow Hydrodynamics (CIFH), is described that is over 500 times faster than conventional time integration techniques. CIFH is a hybrid approach, utilising a combination of pre-computed flows and hydrodynamic equations and allows the efficient simulation of dynamic control systems for the transport of cells through micro-fluidic devices. The speed-ups achieved by using pre-computed CFD solutions mapped to an n -dimensional control parameter space, significantly accelerate the evaluation and improvement of control strategies and chip design. Here, control strategies for a naturally unstable device geometry, the microfluidic cross-slot, have been simulated and optimal parameters have been found for proposed devices capable of trapping and sorting cells.

1 Introduction

Cells are exposed to fluid forces in a variety of physiological contexts,^{1,2} including blood flow, air movement in lung aveoli,^{3–5} and shear stress on cardiomyocytes^{6,7} and platelets.^{8,9} Microfluidic devices, with similar length scales to blood vessels and other biological fluid channels, enable the construction of a customised biomimetic environment in the laboratory. By customising the channel geometry, and hence the fluidic environment of cells, forces can be applied to cells that mimic those encountered *in vivo*.^{10–12} In addition, microchannels can also include features such as constrictions,¹³ precisely tuned outlet sizes,^{14,15} junctions¹⁶ and pillars¹⁷ to direct and sort cells based on their size and behaviour in flow. High throughputs can be obtained by making use of these geometric structures, allowing large numbers of cells to be processed rapidly. However, the force profiles and sorting decisions are static – encoded in the geometry at manufacturing time.

Cells are dynamic, exhibiting both rheological characteristics¹⁸ and active biochemical responses to applied force.¹⁹ The response to externally-applied forces by cells is complex and non-linear, due to interactions between membrane structure, internal

organelles in the cell and viscous behaviour of the internal fluid. Pathological conditions, such as diabetes, modify the biochemical properties of red blood cells, changing the force response.^{20–22} The malaria parasite modifies both the membrane chemistry and the internal structure of red blood cells, causing a dramatic increase in red cell stiffness.^{23,24} Environmental forces also provoke active responses, such as stem cells differentiating;²⁵ blood vessel endothelial cells changing stiffness;²⁶ and healthy cells becoming malignant.^{27,28}

Investigating dynamic behaviour, such as the response to varying forces applied to a cell in realtime, requires active control. Complementary technologies, such as electric fields;^{29,30} magnetism;^{31,32} optical forces;³³ and surface acoustic waves,³⁴ are often used to impose forces on suspended cells in microchannels. In contrast to these technologies, the use of the fluids to directly manipulate cells offers a preparation-free, biomimetic approach with a low risk of cell damage. In addition, the use of direct fluid manipulation allows multiple, independent, fluid control systems to be densely integrated on a single chip.³⁵ However, the interactions between actuators; the control algorithms; the cells under test and the dynamics of the fluid must be characterised in order to develop an efficient controller. Testing and characterisation of control algorithms experimentally is both time consuming and expensive. A large number of iterations is typically required to develop and tune an optimal controller. Not only is this time consuming experimentally, but may also be expensive in terms of reagent and sample costs. This ultimately limits the scope for optimisation and the complexity of systems that can be feasibly attempted. Flow geometry may require refinement

^aDivision of Biological Engineering, Monash University, Melbourne, Australia. E-mail: Andreas.Fouras@monash.edu

^bFluids Laboratory for Aeronautical and Industrial Research (FLAIR), Department of Mechanical and Aerospace Engineering, Monash University, Melbourne, Australia

† Electronic supplementary information (ESI) available: Experimental validation of CFD; movies of cells in a microfluidic device undergoing manipulation due to the control system. See DOI: 10.1039/c1lc20191c

and therefore the manufacture of new prototypes, with the attendant lead times and costs. Therefore, simulation of dynamic microfluidic systems is critical to the development of this field.

The greatest limitation of existing simulation techniques is that the computation time required is prohibitively long. Consequently, control simulations using these techniques are impractical and limit experimentation with control system design; control tuning parameters; and geometry. A common general approach for simulating problems of this nature formulates the system as a set of coupled systems that must be solved iteratively.³⁶ This is known as the *fluid-structure interaction* problem, where the structure in this case is a cell. Using this solution method, the fluid system is initially solved with an initial approximate cell location. The forces resultant on the cell are then calculated and cell deformation is estimated using a finite-element solid mechanics model of the cell. The fluid domain is then re-meshed based on the new cell deformation and a new solution to the fluid system is computed. This process repeats until the error between successive solutions has been reduced significantly.

After the error has reduced, net acceleration of the cell can be computed from the resultant forces and integrated to find an updated cell position. Using a standard numerical quadrature algorithm, such as a fourth-order Runge–Kutta algorithm, the iterative process described earlier must be repeated at least three further times to successfully integrate the acceleration to find an updated position. This process then repeats for every time step. Even for very efficient computational fluid dynamics (CFD) solvers and small solid mechanics models, each iteration step may take many hours on modern computer systems.

However, when the solid body can be described as a simple geometric shape and the flow can be considered to be minimally perturbed by the presence and motion of the solid body, a simplified approach based on the hydrodynamic drag equations can be used. Many cells can be approximated as spheres or ellipsoids and hence lend themselves well to this approach. Recently, this approach was used to model the motion of bacterial cells in a passive microfluidic trap.^{37,38} A background flow was computed for the microfluidic trap geometry and the bacterial motion was computed using hydrodynamics. However, in that study only a steady state flow with static boundary conditions was considered. In this paper, a hybrid approach, using a combination of precomputed flows and hydrodynamic equations is developed, allowing a dynamic control system for cells to be efficiently simulated.

In this study, it is demonstrated that the simulation technique can be used to characterise and design a control system to capture, trap and manipulate cells in a microfluidic cross slot (Fig. 1). First used to study polymer extensional hysteresis,³⁹ the microfluidic cross slot has recently been extended to study polymer beads and cells.⁴⁰ Due to the geometry and fluid boundary conditions in the device, a saddle point is formed in the centre of the channel, resulting in purely extensional flow. This exerts a force on the cell at the centre of the fluid channel, stretching it (Fig. 1a). Once the cell has been captured by the device, the cell can be redirected to one of the two outlets (Fig. 1b). Control over the cell position can be indirectly achieved by modifying the relative flow rates (Fig. 1c).

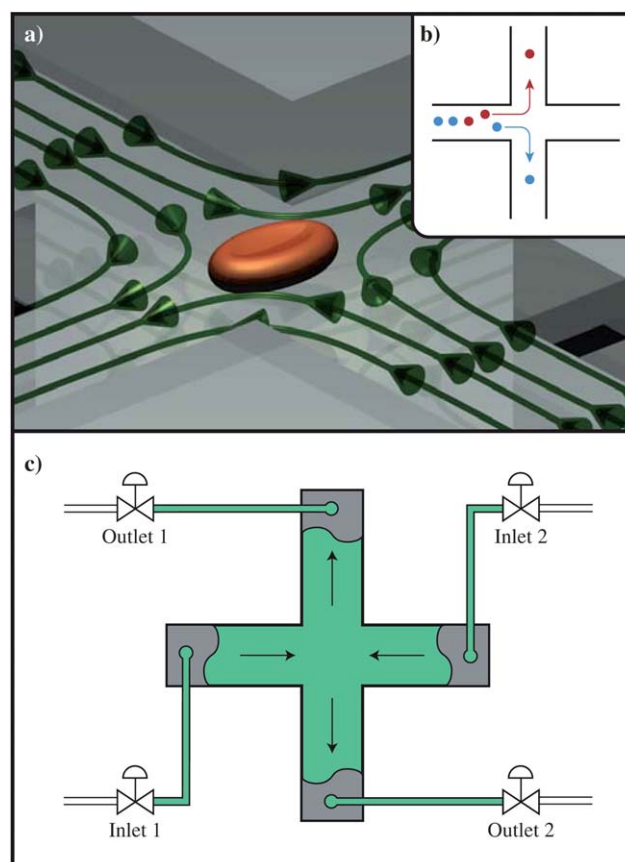


Fig. 1 Stretching (a) and sorting (b) cells using microfluidics. A red blood cell is shown (not to scale) undergoing stretching due to extensional flow. Fluid velocity, as indicated by the streamlines, results in shear stress on the cell; causing it to stretch. Sorting (b) can also be achieved using this device by directing cells toward one of the two outlets. Control of the shear, saddle point position and therefore position of the cell in the microfluidic cross can be effected by changing the relative flow rates of the inlets and outlets (c). For example, a higher relative flow rate through Inlet 1 will result in the saddle point moving to right, relative to the centre of the channel. Shear can be adjusted by modifying the overall flow rate.

2 Methodology

The method proposed in this paper, Computed Interpolated Flow Hydrodynamics (CIFH), significantly reduces the computation time compared to a conventional fluid-structure interaction approach, such that each step can be computed in less than a second. Three primary strategies are employed to achieve this: the motion of the cell is decoupled from the fluid, avoiding the expensive iteration between the fluid and solid mechanics models; the time evolution of the fluid system is treated as a Linear Time Invariant system, allowing flow solutions to be computed ahead of time; and flow solutions are interpolated, allowing the flow parameters to be varied continuously within the solution space.

Fluid-cell coupling

For small Reynolds numbers in the regimes of creeping and Stokes flow ($Re \leq 1$), the expensive computation of

fluid-structure interactions can be reduced to a closed-form equation known as the Bassett-Boussinesq-Oseen equation (BBO).^{41,42} These equations use the hydrodynamic drag of the cell, along with its mass and viscosity to compute the acceleration of the cell in an ambient fluid. Drag correction factors for spherical and aspherical shapes are well-known, allowing great flexibility across a range of cell types without requiring direct computation of the solid mechanics.

Time independence of the fluid system

In the regime of Stokes flow, the inertia terms of the Navier–Stokes equations are negligible. Therefore, the flow solution can be completely described by the geometry and boundary conditions. As inertia is negligible, there is nothing to cause the fluid system to diverge from the time independent steady-state solution for a given input. This is analogous to a Linear Time-Invariant (LTI) system in signal processing theory – for a given input stimulus, the output is always identical, regardless of the time history of the system. As the fluid system is decoupled from the cell solution, the varying location of the cell over time does not change the time invariant properties of the flow. This allows flow solutions to be computed independently of the control simulation.

Interpolation of flow solutions

Finally, the LTI properties of the fluid system are utilised to reduce the number of flow solutions required by the simulation. As any combination of flow parameters (*e.g.*, boundary conditions) could be demanded by the fluid control system, it is necessary to efficiently find the solution to the flow for an arbitrary combination of flow parameters. This is achieved by discretising the flow parameters onto a grid of available solutions and interpolating between these available solutions, yielding an efficient method for generating the required flow solution. As for finite element methods, this method is accurate provided the discretisation is chosen to minimise abrupt changes in the solutions.

The overall process is summarised in Fig. 2. Firstly, a controller (Fig. 2a), which may be any multiple-input multiple-output (MIMO) discrete controller, demands a change to the flow parameters (in this example, flow rates) based on the cell location. Simulations of flow actuator noise and resolution are mixed into the flow parameters at this point. Secondly, the flow parameters are mapped to a grid of available flow solutions (Fig. 2b and inset). Next, the flow solutions closest to the demanded flow parameters are identified (Fig. 2c). These solutions are then interpolated to generate the flow solution for the flow parameters demanded by the controller (Fig. 2d). Finally, the equations describing the cell motion, the BBO equations are integrated to provide the location of the cell for the next time step (Fig. 2e). These processes are discussed in detail in the following sub-sections.

2.1 Flow field generation

Typically, in order to model the response to the changing fluid boundary conditions, a computational fluid dynamics (CFD) solver would be used to predict the flow field at every flow rate

requested by the controller. This is computationally expensive and time consuming, especially when simulating a large number of control scenarios. Even for a two-parameter system, the number of CFD runs required would be large in order to fully cover the space. Instead, in the present approach, the space is sampled and an interpolation approach is used to evaluate the flow field between these sample locations.

Flow solutions are obtained over an n -dimensional grid of the input parameters. The number of input parameters will be largely dictated by the complexity of the flow geometry and the degrees of freedom of the system. These flow solutions can be computed by any means, including a general-purpose CFD solver such as VIPER or FLUENT. As these flow solutions are computed once and then stored for future simulations, subsequent CIFH simulations are very efficient.

Each flow solution is treated as a node on a parameter space grid (see Fig. 2b for a two-dimensional example). In a process analogous to that used by the finite element method, the parameter nodes are meshed to form grid elements (in 2D, these are quadrilaterals). The meshed domain therefore encloses the space of input parameters for which there are solutions available. Any set of valid input parameters will be fully enclosed by exactly one parameter grid element[‡]. The parameter grid can then be efficiently and rapidly searched by an algorithm such as an Alternating Digital Tree.⁴³

During execution of the control simulation, flow parameters demanded by the controller are mapped onto the parameter mesh (see Fig. 2c). The element that encloses these parameters is then identified and linear interpolation is performed between the CFD solutions that comprise the element nodes (Fig. 2d). This is similar to the linear interpolation scheme used in the finite-element method, where the interpolation typically takes place between individual scalars rather than complete solutions.

Finally, to reduce the computational overhead associated with interpolating a number of large meshes, the interpolations are evaluated using a *lazy evaluation* scheme.⁴⁴ Instead of computing the interpolated values for each node in the resulting CFD solution, these values are only computed when needed by the simulation code and then cached in memory until the flow parameters are updated again.

2.2 Cell dynamics

A fourth-order Runge–Kutta integration scheme is used to integrate the cell velocity and hence simulate the evolution of its position over time (Fig. 2e). Provided the dimensions of the microchannel are large relative to the cells under consideration, cell dynamics can be decoupled from the fluid dynamics of the system. Therefore, the evolution of the cell position is independent of the fluid dynamics solutions and changes to the cell position, orientation or shape do not require new flow solutions to be obtained. However, cells will display inertial effects due to finite size and mass. These effects are described by integrating the

[‡] At element intersections, more than one element will enclose the set of input parameters. In this case one is arbitrarily chosen, as the nodes over which the interpolation takes place are identical in the plane of intersection.

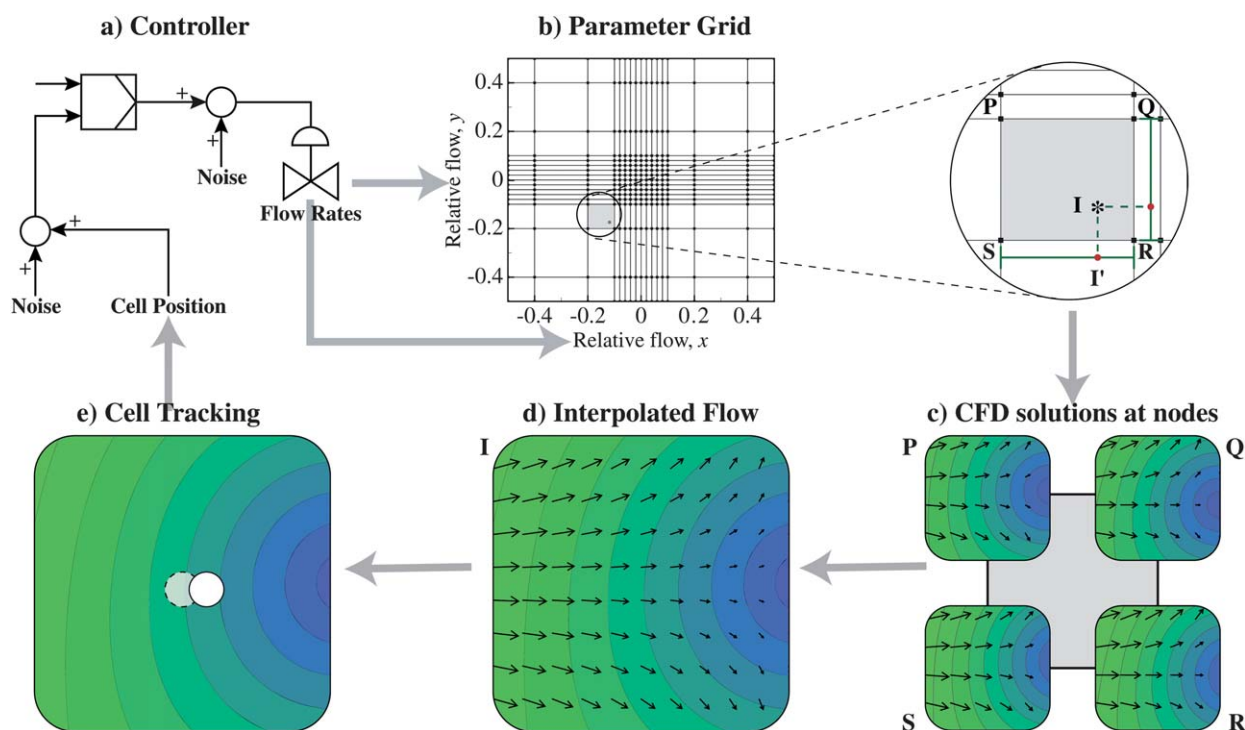


Fig. 2 CIFH control simulation process. A controller uses the cell position as an input to determine a new set of boundary conditions, in this case relative flow rates (a). Available solutions for these boundary conditions are mapped to a parameter grid, in this case with two dimensional, where each dimension relates to a flow rate parameter (b). The point marked with an asterisk (*) indicates the demanded combination of flow rate parameters (shown in the exploded view). The four nodes on the parameter grid forming the element boundary are identified (P,Q,R,S), where each node represents a complete CFD solution (b,c). The four solutions are then interpolated to find the resultant bilinear-interpolated flow (d). Finally, hydrodynamic equations are used to compute the motion of the cell and hence the updated cell position (e).

common hydrodynamic equation for particle drag in a flow, the Bassett-Boussinesq-Oseen equation,⁴²

$$\begin{aligned}
 m_c \frac{d\mathbf{v}}{dt} = & -\frac{1}{2} m_f \frac{d}{dt} \left(\mathbf{v} - \mathbf{u} - \frac{\alpha^2}{10} \nabla^2 \mathbf{u} \right) \\
 & - 6\pi\alpha\mu_f \left(\mathbf{v} - \mathbf{u} - \frac{\alpha^2}{6} \nabla^2 \mathbf{u} \right) \\
 & - \frac{6\pi\alpha^2\mu_f}{\sqrt{\pi}\mu_f} \left(\int_0^t \frac{d}{dt} \left(\mathbf{v} - \mathbf{u} - \frac{\alpha^2}{6} \nabla^2 \mathbf{u} \right) \frac{d\tau}{\sqrt{t-\tau}} \right) \\
 & + (m_c - m_f) \mathbf{g} \\
 & + m_f \frac{D\mathbf{u}}{Dt},
 \end{aligned} \quad (1)$$

where m_c and m_f are the cell and fluid mass, respectively; μ_f is the fluid viscosity; α is the cell radius; \mathbf{g} is the acceleration due to gravity; \mathbf{v} is the cell velocity vector; and \mathbf{u} is the fluid velocity vector. The equation is reduced in complexity by taking into the account the following factors: the Faxen terms ($\nabla^2 \mathbf{u}$) can be neglected when $\alpha/l \ll 1$, where l is the channel length scale, a condition which holds except for very small channels or large cells;⁴² and the integral term (known as the history term) approaches zero for Reynolds numbers less than 1.^{42,45} Additionally, the primary aim in this work is to model scenarios where the cell is already present in the flow and does not start from rest, hence reducing the importance of the history term in this case.

For this analysis, buoyancy is ignored as only the in-plane velocity of the cell within the channel is of interest.

Finally, the sphere drag used for the drag term in (1), *i.e.*

$$F = -6\pi\alpha\mu_f(\mathbf{v} - \mathbf{u}) \quad (2)$$

is substituted for the more general inertial drag equation⁴⁶

$$C_D = \frac{2F}{\rho_f \pi \alpha^2 \|\mathbf{v} - \mathbf{u}\|^2}. \quad (3)$$

This formulation is equivalent to that in (2), but lends itself more readily to describing aspherical shapes such as ellipsoids.⁴⁶ In the examples described in this paper, we employ $C_D = 24/Re_c$ for drag on a sphere at low Reynolds numbers.

Hence, expressing the masses in terms of areal density,

$$\begin{aligned}
 \frac{d\mathbf{v}}{dt} = & -\frac{1}{2} \frac{\rho_f}{\rho_s} \frac{d}{dt} (\mathbf{v} - \mathbf{u}) \\
 & - \frac{1}{2} \frac{\rho_f}{\rho_s} C_D \|\mathbf{v} - \mathbf{u}\| (\mathbf{v} - \mathbf{u}) \\
 & + \frac{\rho_f}{\rho_s} \frac{D\mathbf{u}}{Dt}.
 \end{aligned} \quad (4)$$

Where the cell is known to be undergoing deformation due to fluid forces, the drag coefficient C_D can be additionally varied to simulate the change in hydrodynamic behaviour due to the shape change. The drag correction factors for ellipsoids are well

known,^{42,47} allowing motion of aspherical cells such as red blood cells to be simulated. Additional behaviours are easily integrated into the simulation. For example, red blood cell tumbling,^{48,49} could be simulated by estimating the rotation rate from the capillary number⁴⁹ and applying the appropriate combination of the drag factors for axial- and normal-axis flow around an ellipsoid.⁴²

The BBO equations are also valid for simulations containing a number of cells by approximating the cells as an ensemble of single cells. For practical concentrations of cells, limited by the ability of the imaging system to reliably identify individual cells, this approximation is accurate. Any cell moving through a fluid produces a disturbance field in the fluid. For a single cell, the effect of this disturbance field is compensated for within the BBO equations. However, the effect of disturbance field from neighbouring cells cannot be compensated for. The disturbance field affects the base flow rate by just 10% at a distance of 5 diameters from the cell,⁴⁶ where the cell velocity is similar to the fluid velocity and the fluid and cell densities and viscosities are similar. Hence, the motion of cells for linear concentrations less than or equal to one cell per 5 diameters can be approximated by an ensemble of single cells moving through a fluid with minimal loss of accuracy.

For small cells, it may be important to model particle diffusion. This is a straightforward addition to the overall method, using the random-walk method of Ghoniem,⁵⁰ where particle positions are modified at each time step based on a Gaussian random distribution that is scaled based on the Schmidt number of the particles in the carrier fluid.

2.3 Control system

A simple control algorithm, based on PID (proportional integral derivative) control is used in this paper to control cell position (Fig. 2a). The control algorithm can be defined in terms of a pair of independent one-dimensional PID algorithms (one for each axis of control $-x$ and y), as

$$e = x_s - x_c \quad (5)$$

$$f = K(e + K_D \dot{e} + K_I \int e dt), \quad (6)$$

where e is the error, x_s and x_c are the desired and actual positions of the cell, respectively and K , K_I and K_D are the proportional, integral and differential gains, respectively.

CIFH is not limited to the simulation of PID control algorithms – any discrete control algorithm can be simulated using this method. Additionally, the simulation is efficient enough to be run in realtime inside the control loop for model-based control.

2.4 Actuator modelling

A limitation of the interpolation approach to modelling the change in boundary conditions is that it assumes that a change from one boundary condition to another can be undertaken instantaneously, regardless of the physical plausibility of this. However, for a non-turbulent, viscous flow, the response time of the fluid system will be dominated by the response time of the actuator controlling the fluid flow rate. Hence, fluid response

time is incorporated with the actuator response time to give an effective system response parameter. In this paper, actuator response has been modelled as a first order system, which will exponentially converge on a final value at a rate determined by the system time constant

$$\frac{dq}{dt} = \frac{1}{\tau}(q_{fv} - q), \quad (7)$$

where q is the flow rate, q_{fv} is the final value of the flow rate (the demand flow rate) and τ is the time constant. While a simple first order model has been used, the actuator model can be extended in the general case to a discrete transfer function with higher order responses and incorporate non-linear behaviours such as actuator hysteresis.

A typical practical actuator is also limited by positioning resolution. The sources of error in an actuator may include digitisation resolution and noise; sensor accuracy and the response of the positioning controller. The limiting response of the controller can be modelled by (7). Digitisation noise and resolution are modelled by first quantising the demanded value to the actuator resolution, followed by the addition of zero mean white noise (Fig. 2a), where the noise amplitude is equal to the half the resolution.

2.5 Observer modelling

The behaviour of a limited observer, for example a camera of finite resolution, is also modelled. Positional data into the controller will be limited by the resolution and update rate of the cell position sensor (in many cases, this would be a camera coupled with appropriate software). As there is little benefit in updating the controller parameters faster than input can be obtained from the sensors, the update rate of the sensors is modelled by adapting the controller update rate to be equal to or slower than the projected frame rate of the cell sensor. Resolution is modelled as a digitisation process, similar to the actuator model described previously, with the position obtained from the cell tracking model combined with a white noise process (Fig. 2a) and quantised to the imager resolution.

3 Results and discussion

3.1 Channel geometry

A computational fluid dynamics (CFD) model of the cross slot geometry was constructed, with a nominal channel width of 100 μm . The Reynolds number, as defined by the channel width and the average inlet flow velocity, was 1 for a working fluid of water. By scaling the magnitude of the solutions, flows with lower Reynolds numbers were also generated. A high-order spectral element solver^{51,52} was used to accurately compute the solutions to the flow. Two-dimensional and three-dimensional geometries were solved for, with 3D aspect ratios between 0.75 and 2. For aspect ratios above 1 (channel height equal to channel width), the flow approached the two-dimensional result and the out-of-plane velocity was minimal.

As stated in §2.1, a parameter space grid of the possible solutions is needed to efficiently generate flow fields for the control system. A non-dimensional parameter for the ratio of the flow velocities between the two opposing inlets was defined

$$f_x = \frac{v_1 - v_2}{v_1 + v_2}, \quad (8)$$

where v_1 and v_2 are the average inlet flow velocities for inlets 1 and 2, respectively (see Fig. 1c). The flow rate deviation can be defined similarly for the two opposing outlets.

CFD solutions for over 350 combinations of inlet and outlet parameters were computed. The two dimensional location of the saddle point was used to map the change in the characteristics of the flow with respect to the input parameters. In each case, the saddle point position was identified using an automated Levenberg-Marquardt optimisation scheme,^{53,54} whereby a conic section was fitted to the velocity magnitude field in the approximate vicinity of the saddle point. Validation was performed using an experimental flow model and PIV (particle image velocimetry).^{55,56} Flow velocity fields show excellent agreement at a number of saddle point locations (comparisons for saddle points at (0,0); and (0,20) are given in the ESI†). The relationships between the relative inlet flows and saddle point for CFD and PIV showed good qualitative agreement. In both cases, the change in saddle point position and flow structures had a piecewise linear relationship, demonstrating that bilinear interpolation can be used to accurately obtain solutions for any combination of f_x and f_y within the solution space (Fig. 2).

3.2 Trapping simulation

Using the CIFH method, the speed and repeatability of cell capture and the stability of a cell trap based on a cross-flow geometry can be assessed in a computationally efficient manner. Cells enter from one of the inlets, in this case inlet 1 (Fig. 1c), and are assumed to be suspended in solution. Injection of cells into the fluid is not simulated, rather it is assumed that the cells were previously prepared and suspended in the working fluid prior to device activation or mixed into the working fluid *in situ* using an upstream T- or oscillatory-mixer.¹⁶ In either case, the location of the cells within the channel as they are transported by the working fluid is randomised – only a very small percentage of the cells will be transported along the channel centreline. In the case of healthy red blood cells, a parabolic distribution is expected.⁵⁷ Hence, to investigate the ability of the system to successfully trap an arbitrary cell that is transported into the device, the control response was simulated with an initial cell position 15 μm away from the centreline.

Fig. 3 shows the control response of the cell as it moves to the saddle point in the centre of the channel for an idealised and two non-ideal cases (a short video of each case is also available in the ESI†). Simulation parameters were chosen to model a red blood cell in the flow, where an average red blood cell is assumed, filled predominately with solution similar to water and of radius 4 μm . Relevant parameters for simulation cases I–III are summarised in Table 1.

Increasing noise and decreasing observer resolution affects both the stability of the final trap and the time to achieve a stable trap. As resolution decreases and actuator noise increases, oscillatory behaviour becomes more prevalent. However, the overall noise remains low, due to the relative size of the cell and low flow velocities. Even in the low resolution and high noise case (Case III), position noise is much less than 1 μm . This is due to the presence of digitisation noise – the long-term average of the

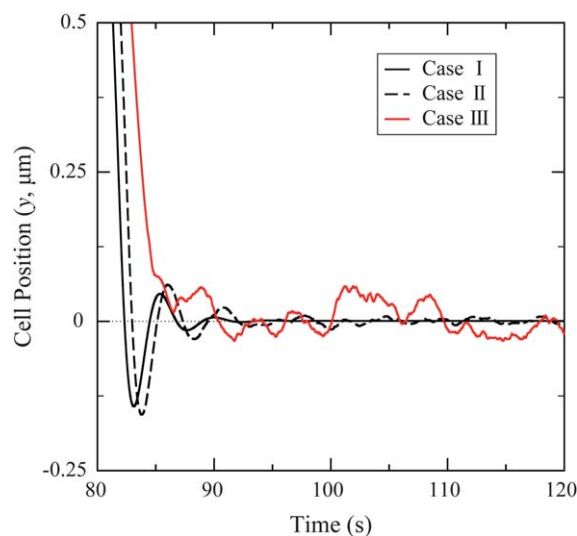


Fig. 3 Controlling the position of the cell using fluid flow. By adjusting the relative flow rates in the device, and therefore moving the saddle point, the flow velocity can be used to direct the cell. Based on this principle, a feedback control system can be used to position the cell and stabilise the system. Response curves show the y (vertical) position of the cell vs. time for case I (solid line); case II (dashed line) and case III (grey line).

Table 1 Parameters chosen for the trapping simulations (§3.2)

Simulation Parameter	Case I	Case II	Case III
Imaging rate	200fps		
Cell radius	4 μm		
Cell:Fluid density ratio	1 : 1		
Initial y location of cell		15 μm above centre line	
Proportional gain, x	0.2		
Proportional gain, y	1.25		
Channel Width	100 μm		
Average flow velocity	1 $\mu\text{m s}^{-1}$		
Reynolds number	0.1×10^{-3}		
Observer resolution	Ideal	0.1 μm	1 μm
Actuator noise	None	None	1%
Actuator time constant	0	50ms	100ms

observed location after quantisation will approach the true value, resulting in a stable trap as long as the cell velocities are sufficiently small relative to the acquisition rate. Larger time constants increase the time required to trap the cell, largely due to the increased time required to initially change the flow rates when the control system is activated. An increase of the actuator time constant from 50 ms to 100 ms is sufficient to increase the overall system damping such that the response moves from an underdamped response and begins to approach an overdamped response, further lengthening the trapping time.

3.3 Gain optimisation

For a number of imaging applications, it is important to minimise oscillation of the cell position. Any small movement of the cell will raise the effective noise floor of the image analysis. Additionally, in situations where a secondary high-resolution camera is used to analyse the cell image, it may be necessary to

maintain the cell position within a small region of the channel, as the secondary camera may have a much smaller field of view than the imaging device used for control feedback. In the absence of a closed-form solution for the control response and therefore for the RMS error, non-linear optimisation techniques provide a route to optimisation of the control gains. In this paper, the simulation technique is used to map the space of potential solutions and therefore locate the region of lowest RMS error. This kind of optimisation could also be performed online using an adaptive gain estimation technique.⁵⁸

Over 180 simulations were run, varying the proportional gain in the x and y directions. Due to the computational efficiency of the CIFH technique, these simulations took less than 2 h to complete on a modern multi-core system, corresponding to around 10 CPU-minutes (the product of the number of CPUs and the total runtime of the simulation) per simulation. This contrasts with the time required to generate the CFD data for the parameter space, which was in excess of 42 CPU-days. Therefore, the CIFH technique decreases the simulation time by more than 500 times, once the initial dataset has been generated.

The control system in each case was configured to stably trap the cell while maintaining a mean flow velocity of $10 \mu\text{m s}^{-1}$ ($\text{Re} \approx 1 \times 10^{-3}$) in the inlet channels; after 20 s of trapping the cell, the overall flow rates were increased to a mean flow velocity of $100 \mu\text{m s}^{-1}$ ($\text{Re} \approx 10 \times 10^{-3}$); the cell was maintained in the trap for a further 20 s before the simulation was terminated. Fig. 4a shows a contour of the RMS error of the final 20 s ($v_{\text{avg}} = 100 \mu\text{m s}^{-1}$) of the simulation for each solution. Results for proportional gains in the y -direction less than 0.04 are not shown as they did not result in stable cell trap.

As expected, there is a combination of proportional gains where the error norm is minimised. Additionally, the error in the y axis is strongly dependent on the gain in the x direction, demonstrating that the control in the two axes cannot be considered linear and separable systems. Further improvement of the steady state error can be achieved with addition of differential gain. Fig. 4b shows the variation of the error with varying differential gains in both directions, with the proportional gains fixed at 0.06. By selecting gains that minimise the error, for example $K_{Dx} = 0.25$, $K_{Dy} = 0.2$ the steady state error norm reduces from $0.75 \mu\text{m}$ (proportional-only case) to $0.25 \mu\text{m}$ (proportional and derivative control).

3.4 Cell sorting

The modelling technique described in this paper can also be applied to a simple cell sorting device. The geometry developed previously is used to simulate sorting of cells into two groups. A hypothetical device, based on this geometry, with a camera located above the left hand inlet channel (see Fig. 1b) is presented. A number of metrics could be used to identify and categorise the cell, including diameter, shape, or fluorescent response. Using these metrics, the cell would be placed into one of two categories, corresponding to the fluid outlet to which the cell should be directed. For this scheme to be effective, the concentration of the cells in suspension must be low enough so that the fluid forces applied to one cell do not cause the next cell in suspension to flow towards the wrong outlet. The simulator was therefore used to determine the relationship between

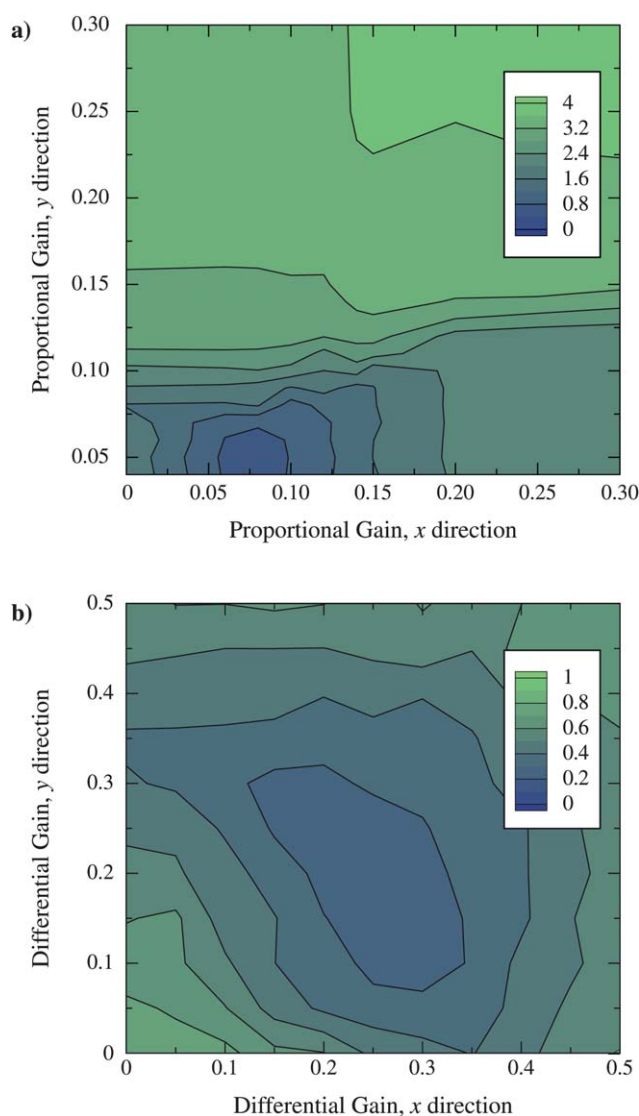


Fig. 4 The steady state error norm as a function of various PID gains. The control system sampling rate was fixed at 100Hz and the flow rate was $100 \mu\text{m s}^{-1}$. (a) Error as a function of proportional gains in the x and y directions. Data for $K_y < 0.04$ is not shown as the system was not stable. There is a clear region of stability and low error for $0.05 \leq K_x \leq 0.12$ and $0.04 \leq K_y \leq 0.08$. (b) Error as a function of differential gains in the x and y directions. For this study the proportional gains were fixed at $K_x = 0.06$ and $K_y = 0.06$.

concentration and accuracy. Parameters for this simulation are summarised in Table 2. Channel dimensions and geometry are the same as those discussed in §3.1. As with the previous simulations, a $4 \mu\text{m}$ red blood cell was simulated for both cell types. A practical sorting device based on these parameters could be used for sorting red blood cells based on their calcium-dependent fluorescence properties.⁵⁹

A number of simulation runs were performed, with 200 cells sorted in each run. Each cell was arbitrarily assigned a cell type, either alternating between ‘type 0’ and ‘type 1’ or randomly distributed. To simulate a fixed cell identification time, the cell type is not assigned until the cell is $50 \mu\text{m}$ from the centre of the channel. At the conclusion of each run, the cell type was

Table 2 Parameters chosen for the sorting simulations (§3.4)

Simulation Parameter	Value
Imaging rate	200fps
Cell radius	4 μm
Cell:Fluid density ratio	1 : 1
Initial y location of cell	Near centre line
Proportional gain, x	None (no control of x axis)
Proportional gain, y	0.8
Differential gain, y	0.05
Channel width	100 μm
Average flow velocity	10 $\mu\text{m s}^{-1}$
Reynolds number (water)	1×10^{-3}
Observer resolution	0.1 μm
Actuator noise	None
Actuator time constant	100ms

compared with the outlet port where the cell exited the fluid domain. The percentage of cells that exited through the correct outlet was used as a measure of the sorting success rate. Cells were inserted into the flow by the simulator at an number of different average injection rates. These injection rates were varied with a Gaussian distribution, with a standard deviation of 10% of the mean, to model the uncertainty present in a real dilution or injection scheme. A number of average rates, from one cell every 20 μm up to one cell every 80 μm , were simulated.

The resulting cell sorting success rates are shown in Fig. 5. For each cell concentration, 200 cells were simulated with an alternating distribution of cell types, representing the worst case, and a further 400 cells were simulated with a random distribution, representing the more common case. Excellent accuracy (95%) is achieved with a mean distance between cells of 75 μm and above. By factoring in the expected accuracy of the imaging system in correctly identifying a given cell type, the overall system accuracy

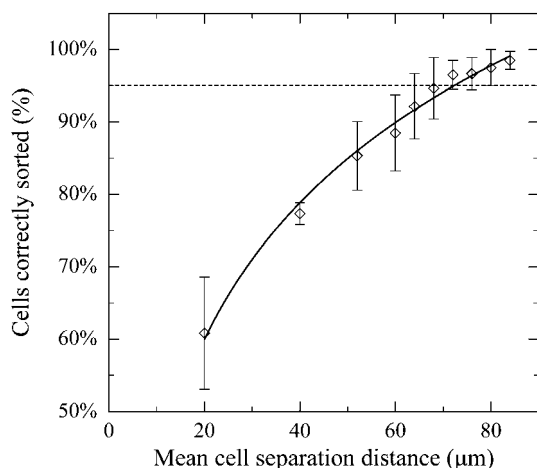


Fig. 5 Cell sorting using the cross geometry. Cells injected from the left inlet are arbitrarily and randomly assigned a type, and are then directed to the upper or lower outlet based on this type. Here the simulation is used to predict the probability that a given cell, assumed to be correctly identified, is directed to the correct outlet in the channel. Error bars indicate the range of values the tests performed, and the results have been fitted to a logarithmic function ($r^2 = 0.99$). The average flow velocity at the inlets is 10 $\mu\text{m s}^{-1}$. Over 95% accuracy is achieved if the cells are spaced at least 75 μm apart.

of a fluid-based cell sorting design can be estimated. This allows the system to be optimised for the throughput and accuracy demands of a given application.

4 Conclusion

An efficient, accurate and flexible method for simulating the control of suspended cells in microfluidic systems has been presented. It is expected that this method, CIFH, will have wide applicability in the design of new and sophisticated feedback control systems for microchannels. As the control simulation is based on a discrete time stepping method, a large number of existing control algorithms and techniques can be simulated using this technique. The method can take advantage of any flow solver, allowing the use of complex flow geometries. Careful choice of the parameter space and refinement of the parameter grid can be used to improve accuracy in cases where the CFD solutions become non-linear with respect to the control parameters. Additionally, the simple actuator models presented in this paper can be extended with measured transfer functions and hysteresis effects of real actuators to simulate the real world behaviour of complex systems.

Compared with earlier, conventional techniques, large improvements in the speed of the simulation have been demonstrated. These efficiency gains have been effected by employing three primary strategies: decoupling cell motion from the flow solver; using an LTI model to represent the change in flow boundary conditions over time; and interpolating between similar flow fields over multiple degrees of freedom. For the data presented in this paper, the generation of CFD flow fields took 42 CPU-days to complete, whereas a typical control simulation, such as those discussed in §3.3 takes under 10 CPU-minutes. Conservatively, the speed-up is well over 500 times when compared to a time-stepping CFD method.

The CIFH control simulation method has been demonstrated, by way of example, using a microfluidic cross slot. It has been shown that active PID control can be used to stabilise and capture a cell in the centre of the microchannel. Secondly, the efficiency of the technique allowed an exhaustive study of the control gain space to be performed to determine the optimal gains to minimise error. Finally, a proposed device for cell sorting has been investigated and the effectiveness of sorting quantified.

References

- 1 A. Fouras, M. J. Kitchen, S. Dubsy, R. A. Lewis, S. B. Hooper and K. Hourigan, *J. Appl. Phys.*, 2009, **105**, 102009.
- 2 R. A. Jamison, J. A. Armitage, J. Carberry, M. J. Kitchen, S. B. Hooper and A. Fouras, *Under Consideration for Current Pharmaceutical Biotechnology*, 2011.
- 3 M. Liu, A. K. Tanswell and M. Post, *Am. J. Physiol. Lung Cell. Mol. Physiol.*, 1999, **277**, L667–683.
- 4 H. R. Wirtz and L. G. Dobbs, *Respir. Physiol.*, 2000, **119**, 1–17.
- 5 M. L. Siew, M. J. Wallace, M. J. Kitchen, R. A. Lewis, A. Fouras, A. B. te Pas, N. Yagi, K. Uesugi, K. K. W. Siu and S. B. Hooper, *J. Appl. Physiol.*, 2009, **106**, 1888–1895.
- 6 J. R. Hove, R. W. Koster, A. S. Forouhar, G. Acevedo-Bolton, S. E. Fraser and M. Gharib, *Nature*, 2003, **421**, 172–177.
- 7 J. C. Culver and M. E. Dickinson, *Microcirculation*, 2010, **17**, 164–178.

- 8 W. S. Nesbitt, E. Westein, F. J. Tovar-Lopez, E. Tolouei, A. Mitchell, J. Fu, J. Carberry, A. Fouras and S. P. Jackson, *Nat. Med.*, 2009, **15**, 665–673.
- 9 E. Tolouei, C. J. Butler, A. Fouras, K. Ryan, G. J. Sheard and J. Carberry, *Ann. Biomed. Eng.*, 2011, **39**, 1403–1413.
- 10 S. S. Lee, Y. Yim, K. H. Ahn and S. J. Lee, *Biomed. Microdevices*, 2009, **11**, 1021–1027.
- 11 M. Rossi, R. Lindken, B. P. Hierck and J. Westerweel, *Lab Chip*, 2009, **9**, 1403.
- 12 F. J. Tovar-Lopez, G. Rosengarten, E. Westein, K. Khoshmanesh, S. P. Jackson, A. Mitchell and W. S. Nesbitt, *Lab Chip*, 2010, **10**, 291–302.
- 13 R. A. Jamison, S. Dubsy, K. K. W. Siu, K. Hourigan and A. Fouras, *Ann. Biomed. Eng.*, 2011, **39**(6), 1643–1653.
- 14 S. Tan, L. Yobas, G. Lee, C. Ong and C. Lim, *Biomed. Microdevices*, 2009, **11**, 883–892.
- 15 H. W. Hou, A. A. S. Bhagat, A. G. Lin Chong, P. Mao, K. S. Wei Tan, J. Han and C. T. Lim, *Lab Chip*, 2010, **10**, 2605.
- 16 A. Neild, T. W. Ng, G. J. Sheard, M. Powers and S. Oberti, *Sens. Actuators, B*, 2010, **150**, 811–818.
- 17 G. Mahmud, C. J. Campbell, K. J. M. Bishop, Y. A. Komarova, O. Chaga, S. Soh, S. Huda, K. Kandere-Grzybowska and B. A. Grzybowski, *Nat. Phys.*, 2009, **5**, 616–612.
- 18 C. Lim, E. Zhou and S. Quek, *J. Biomech.*, 2006, **39**, 195–216.
- 19 D. E. Jaalouk and J. Lammerding, *Nat. Rev. Mol. Cell Biol.*, 2009, **10**, 63–73.
- 20 C. Le Dévéhat, M. Vimeux and T. Khodabandehlou, *Clin. Hemorheol. Microcirc.*, 2004, **30**, 297–300.
- 21 E. J. Diamantopoulos, C. Kittas, D. Charitos, M. Grigoriadou, G. Ifanti and S. A. Raptis, *Horm. Metab. Res.*, 2004, **36**, 142–147.
- 22 H. Jin, X. Xing, H. Zhao, Y. Chen, X. Huang, S. Ma, H. Ye and J. Cai, *Biochem. Biophys. Res. Commun.*, 2010, **391**, 1698–1702.
- 23 C. T. Lim, *J. Biomech. Sci. Eng.*, 2006, **1**, 82–92.
- 24 A. G. Maier, B. M. Cooke, A. F. Cowman and L. Tilley, *Nat. Rev. Microbiol.*, 2009, **7**, 341–354.
- 25 K. C. Clause, L. J. Liu and K. Tobita, *Cell Commun. Adhes.*, 2010, **17**, 48–54.
- 26 S. McCue, S. Noria and B. L. Langille, *Trends Cardiovasc. Med.*, 2004, **14**, 143–151.
- 27 S. Kumar and V. Weaver, *Cancer Metastasis Rev.*, 2009, **28**, 113–127.
- 28 D. T. Butcher, T. Alliston and V. M. Weaver, *Nat. Rev. Cancer*, 2009, **9**, 108–122.
- 29 M. J. Fulwyler, *Science*, 1965, **150**, 910–911.
- 30 A. Bhagat, H. Bow, H. Hou, S. Tan, J. Han and C. Lim, *Med. Biol. Eng. Comput.*, 2010, **48**, 999–1014.
- 31 S. Miltenyi, W. Müller, W. Weichel and A. Radbruch, *Cytometry*, 1990, **11**, 231–238.
- 32 R. C. Spero, L. Vicci, J. Cribb, D. Bober, V. Swaminathan, E. T. O'Brien, S. L. Rogers and R. Superfine, *Rev. Sci. Instrum.*, 2008, **79**, 083707–7.
- 33 J. Guck, R. Ananthakrishnan, H. Mahmood, T. J. Moon, C. C. Cunningham and J. Käs, *Biophys. J.*, 2001, **81**, 767–784.
- 34 T. Franke, S. Braunmüller, L. Schmid, A. Wixforth and D. A. Weitz, *Lab Chip*, 2010, **10**, 789.
- 35 M. S. Munson, J. M. Spotts, A. Niemistö, J. Selinummi, J. G. Kralj, M. L. Salit and A. Ozinsky, *Lab Chip*, 2010, **10**, 2402.
- 36 J. O. Barber, J. P. Alberding, J. M. Restrepo and T. W. Secomb, *Ann. Biomed. Eng.*, 2008, **36**, 1690–1698.
- 37 M. Kim, Z. Wang, R. H. W. Lam and T. Thorsen, *J. Appl. Phys.*, 2008, **103**, 044701.
- 38 M. Kim and C. Klapperich, *Lab Chip*, 2010, **10**, 2464.
- 39 C. M. Schroeder, H. P. Babcock, E. S. G. Shaqfeh and S. Chu, *Science*, 2003, **301**, 1515–1519.
- 40 M. Tanyeri, E. M. Johnson-Chavarría and C. M. Schroeder, *Appl. Phys. Lett.*, 2010, **96**, 224101.
- 41 M. R. Maxey, *Phys. Fluids*, 1983, **26**, 883.
- 42 E. E. Michaelides, *Particles, bubbles & drops: their motion, heat and mass transfer*, World Scientific, 2006.
- 43 J. Bonet and J. Peraire, *Int. J. Numer. Methods Eng.*, 1991, **31**, 1–17.
- 44 F. Burton and M. Huntbach, *IEEE Comput. Graphics Appl.*, 1984, **4**, 28–33.
- 45 D. J. Vojir and E. E. Michaelides, *Int. J. Multiphase Flow*, 1994, **20**, 547–556.
- 46 F. M. White, *Viscous fluid flow*, McGraw-Hill, 1991.
- 47 D. R. Breach, *J. Fluid Mech.*, 1961, **10**, 306–314.
- 48 Y. Sui, H. T. Low, Y. T. Chew and P. Roy, *Phys. Rev. E: Stat., Nonlinear, Soft Matter Phys.*, 2008, **77**, 016310.
- 49 K. Tsubota and S. Wada, *Phys. Rev. E: Stat., Nonlinear, Soft Matter Phys.*, 2010, **81**, 011910.
- 50 A. F. Ghoniem and F. S. Sherman, *J. Comput. Phys.*, 1985, **61**, 1–37.
- 51 G. J. Sheard, T. Leweke, M. C. Thompson and K. Hourigan, *Phys. Fluids*, 2007, **19**, 083601.
- 52 G. J. Sheard, *Journal of Fluids and Structures*, 2011, DOI: 10.1016/j.jfluidstructs.2011.02.005, **In Press**.
- 53 K. Levenberg, *Q. Appl. Math.*, 1944, **2**, 164–168.
- 54 D. W. Marquardt, *SIAM J. Appl. Math.*, 1963, **11**, 431–441.
- 55 A. Fouras, D. Lo Jacono and K. Hourigan, *Exp. Fluids*, 2007, **44**, 317–329.
- 56 A. Fouras, D. Lo Jacono, C. V. Nguyen and K. Hourigan, *Exp. Fluids*, 2009, **47**, 569–577.
- 57 G. Mchedlishvili and N. Maeda, *Jpn. J. Physiol.*, 2001, **51**, 19–30.
- 58 K. J. Åström and T. Hägglund, *Advanced PID Control, Instrumentation, Systems, and Automation Society*, 1st edn, 2006.
- 59 L. Kaestner, W. Tabellion, E. Weiss, I. Bernhardt and P. Lipp, *Cell Calcium*, 2006, **39**, 13–19.